IEEE Access
Multidisciplinary | Rapid Review | Open Access Journal

Received 4 February 2023, accepted 28 February 2023, date of publication 9 March 2023, date of current version 15 March 2023.

Digital Object Identifier 10.1109/ACCESS.2023.3254914

RESEARCH ARTICLE

Common Diagnosis Approach to Three-Class Induction Motor Faults Using Stator Current Feature and Support Vector Machine

KENICHI YATSUGI[1], SHRINATHAN ESAKIMUTHU PANDARAKONE[1], YUKIO MIZUNO[1], (Member, IEEE), AND HISAHIDE NAKAMURA[2], (Member, IEEE)

[1]Nagoya Institute of Technology, Nagoya, Aichi 466-8555, Japan
[2]TOENEC Corporation, Nagoya, Aichi 457-0819, Japan

Corresponding author: Kenichi Yatsugi (cng53001@ict.nitech.ac.jp)

ABSTRACT Induction motors are becoming crucial components in numerous industries. The daily usage of induction motors creates the demand for proper maintenance and slight fault detection to avoid serious damage to the induction motor and the shutdown of industries. Among the various kinds of faults in induction motors, bearing faults, broken rotor bar faults, and short-circuit insulation faults are the most common. Thus, detection and classification of these faults in initial stage are attracting great attention. There are conventional methods for detecting such faults, such as the vibration method for bearing faults, the self-organizing map in the case of broken rotor bar faults, and motor current signature analysis for short-circuit insulation faults. From an industrial point of view, diagnosis methods that can classify all these major faults are required. However, reports on the detection and classification of these faults in initial stage using common diagnosis methods are scarce. In this paper, all three kinds of notable faults in an induction motor were artificially induced, and diagnoses using motor stator current spectral features and the rotation speed of the motor were performed. The diagnosis was accomplished using an auto-tunable and arbitrary featured support vector machine algorithm. Although the faults were minor, a high accuracy rate was obtained. The capability to classify the faults and the high diagnosis accuracy prove the robustness and high sensitivity of the method, enabling its practical applications in industries.

INDEX TERMS Bearing fault, diagnosis, insulation fault, rotor bar fault, induction motor, support vector machine.

I. INTRODUCTION

Diagnosis plays an important role not only in the medical and bioengineering fields but also in the fields of the motor industry. Among various available motors, induction motors (IMs) are still considered to be the most reliable and in demand machines. The wide range of use of IMs in the electrical, mechanical, and automobile sectors and their various advantages such as low maintenance requirements, robust construction, inexpensive availability, highly efficient operation, and high adaptability for various load conditions necessitate diagnosis as part of maintenance. Moreover, IMs can be used in harsh environments because of their high robustness. However, because of continuous operations and harsh operating environments, IMs often lead to critical breakdowns due to even minor faults. These IM breakdowns should be prevented at slight fault stages because they may result in extra maintenance work or fatal effects on the entire industrial system. Thus, the demand for fault detection in initial stages is high and increasing to prevent the breakdown and extend the usage time of IMs.

Figure 1(a) and (b) shows the occurrence percentage of the possible class of faults in IMs and the components in an IM, respectively. The faults of IMs are mainly classified into two categories: electrical and mechanical faults [1], [2], [3]. Among the possible classes of faults of IMs, bearing

The associate editor coordinating the review of this manuscript and approving it for publication was Sinisa Djurovic.

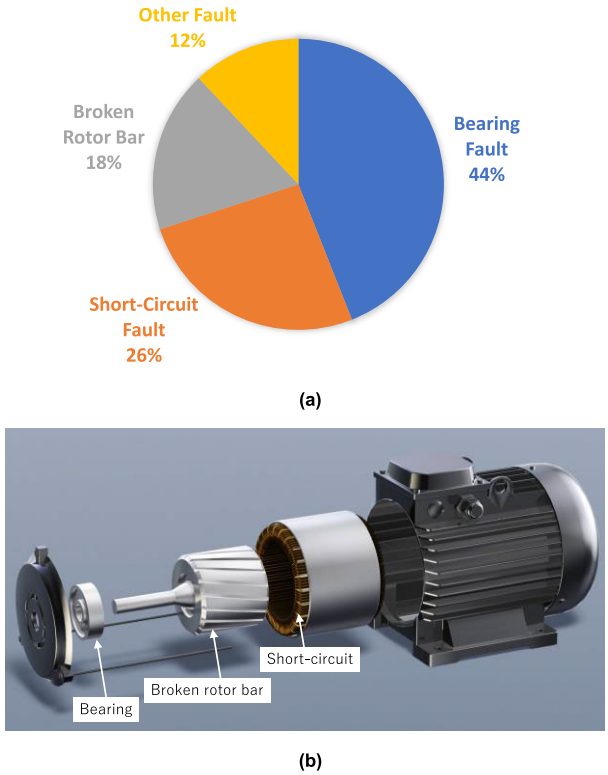

FIGURE 1. (a) Occurrence percentage of possible classes of faults in an induction motors. (b) Class of faults in an induction motors.

faults (44%) has the highest occurrence percentage, followed by short-circuit stator winding faults (26%), broken rotor bar faults (18%), and other kinds of faults (12%) [4]. The main causes of bearing faults are environmental conditions, voltage fluctuations, contamination, and insufficient lubrication [5]. Meanwhile, short-circuit faults are caused by the frequent start/stop of IMs, thermal deterioration due to high temperatures, temperature rise through dust attachment to the cooling fan, moisture absorption, and contact of rotor iron and stator winding. In the case of broken rotor bars, the reason is primarily overheating due to the continuous operation of a motor. From the above three major faults, the common point stands to be the continuous operation of IMs, and considering its fatal impact, these faults should be identified at slight fault stages. However, we cannot practically forecast the fault that may occur. Thus, a common diagnosis method is in demand for distinguishing the various types of slight faults.

Some experimental and diagnosis results for short-circuit faults, bearing faults, and broken rotor bars are discussed below. Short-circuit faults stand to be a crucial fault because they only cause insignificant changes in the magnitude of the phase current. The most common diagnosis methods used in this regard are the park vector method [6], partial discharge characteristics method [7], [8], [9], and load current methods [10], [11]. Previous results found that two or more turn-to-turn short circuits could be easily diagnosed with practically acceptable accuracy. However, distinguishing winding with one-turn-to-turn short-circuit fault from healthy winding is still challenging.

In the case of broken rotor bar faults, the following studies have been conducted [12], [13], [14], [15], [16], [17]. For instance, for detecting the geometrical asymmetry of a rotor caused by the breakage of a bar(s), the method using sideband components has been widely studied. The sideband components appear below and above the fundamental component in the frequency spectrum of the load current. However, this method has drawbacks in identifying slight faults. Recently, characteristic frequencies and the self-organizing map [18] have been used in detecting broken rotor bar faults by using the amplitude of the characteristic frequency components of the load current spectrum as features [19]. However, the diagnosis results show the same less accuracy rate in the case of slight fault detection in rotor bars.

For the bearing faults of IMs, various diagnosis methods have recently been proposed, including vibration [20], [21], [22], acoustic emission [23], [24], [25], stray flux monitoring [26], [27], and motor current signature analysis (MCSA) [28], [29], [30], [31], [32], [33]. Although the vibration and acoustic emission methods are effective in detecting faults, those methods are sometimes unsuitable for practical use because vibration and acoustic sensors can detect ambient noise. For flux monitoring methods, there can be an implementation limitation of flux sensors in practical systems. Meanwhile, MCSA is easy to implement, robust to ambient noise, and has cost-effective maintenance.

Until now, each fault is diagnosed using several methods, and finding a common diagnosis method to solve all three major faults at the initial stage is a challenging point. On the other hand, there have been recent reports on diagnosis for distinguishing multiple kinds of faults using MCSA. In [34], the multiple-fault diagnosis of unbalanced shaft rotation, bearing fault, and broken rotor bar using the combination of the stator current and vibration signals has been reported. The MCSA method for multiple faults including broken rotor bars and short circuits has also been applied previously [35]. However, reports on the detection and classification of these major faults in the slight fault stage using common diagnosis methods are scarce because of the sensitivity and implementation difficulties of such faults. In [36], the vibration signal is combined with MCSA to increase its sensitivity in distinguishing the class of faults. In the MCSA method, the degree of faults is primarily identified. However, the challenge of identifying slight faults still exists.

Apart from the various analysis methods for detecting motor fault, the machine learning (ML) algorithm is effective for the high sensitivity diagnosis of faults of IMs. The above major faults have been diagnosed with the help of the ML algorithm, such as by combining the motor current spectral components with support vector machine (SVM) and k-NN [36], [37]. However, a common diagnosis method for classifying all three major faults (short-circuit faults, bearing faults, and broken rotor bars) and the possibility of classifications in slight fault stages have never been reported.

In this study, the three major faults of IMs are diagnosed using the combination of the load current spectra and SVM.

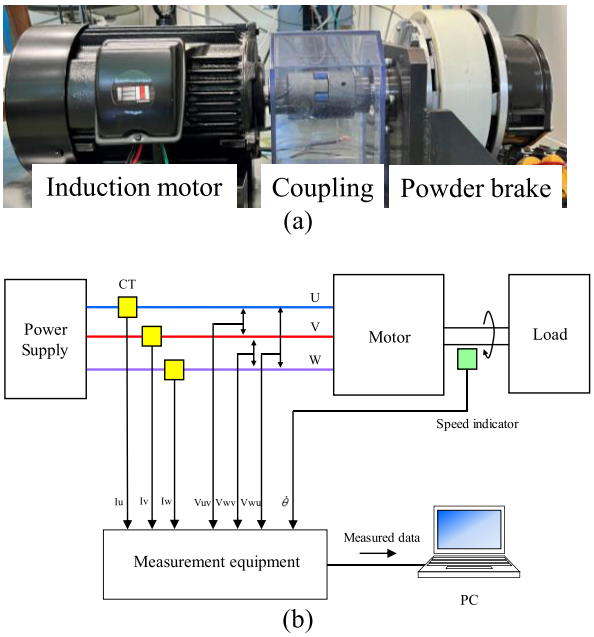

FIGURE 2. Experimental setup. (a) Induction motor setup. (b) Measurement system.

The purpose of the study has three main points: (1) determining a common method for identifying all three majors faults, (2) identifying faults at slight fault stages, and (3) distinguishing not only the faulty motor from the healthy motor but also the faults among the IMs. In this diagnosis, the sideband components of the load current spectra are used as features of the SVM, where the motor rotation speed is used as an additional feature. The results show that the method discussed is effective in identifying all three major faults.

II. EXPERIMENTAL SETUP AND INTRODUCTION OF FAULTS

The experimental setup is shown in Figure 2. A four-pole three-phase IM (2.2 kW, 200 V, 8.5 A) was used as a specimen. A powder brake (Mitsubishi, ZKB-5HBN) was coupled to the IM as a load. The rotation speeds were adjusted to 1765, 1770, 1775, and 1780 min^{-1} by using the powder brake. The load current, line-to-line voltage, and rotation speed were monitored using current sensors (HIOKI, 9695-02), voltage sensors (HIOKI, 9666), and a tachometer (ONOSOKKI, HT-5500), respectively. The measured data from these sensors were sent to a desktop computer in less than 20 seconds using a serial-based communication system through a measurement equipment developed by the authors. The measurement equipment had 8 channels and 8 analog-to-digital (A/D) converters. A field programmable gate array controls 3 A/D converters with a sampling time selection of 10 μs. Totally, 7 channels were used; one for rotation speed, and 3 for each current and voltage, respectively. The full-scale current and voltage measurements are 20 A, and 700 V. A data transfer software was created in Visual C++ language. Data were recorded every 30 s, and the data length was 2^{17}. The sampling time is chosen to obtain the appropriate frequency resolution (0.76 Hz) and so that the differences in the spectra between healthy and faulty cases are distinguished. The AC power supply frequency to the IM was 60 Hz.

TABLE 1. Dimension of the bearing and the rotor.

	Specification	Dimension
Bearing	Inner diameter	25 mm
	Outer diameter	52 mm
	Width	15 mm
Rotor	Diameter	100 mm
	Rotor bar length	128 mm
	Rotor bar diameter	Approx. 5 mm
	Number of rotor bars	28

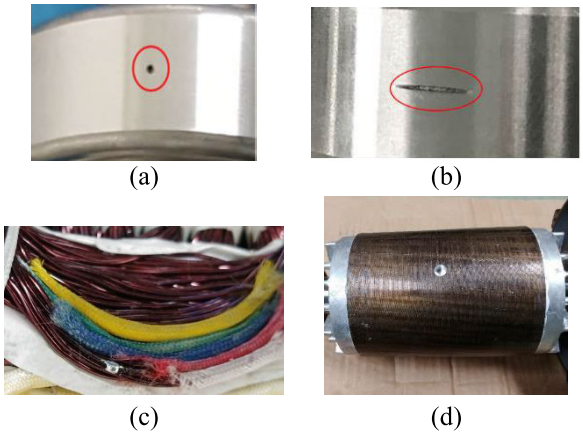

FIGURE 3. Artificially introduced faults. (a) Hole fault on the bearing. (b) Scratch fault on the bearing. (c) Short circuit of the winding. (d) Broken rotor bar.

The slight bearing, short-circuit faults, and broken rotor bars in IMs were introduced artificially because collecting such faults from factories was complicated. In the case of the bearing fault, a hole or a scratch was introduced on the outer diameter surface of the outer ring of the bearings. Deep groove ball bearings (NSK, 6205ZZCM) were used as specimens. The dimensions of the bearing are shown in Table 1. The diameter and depth of the hole were 0.5 mm. The length, width, and depth of scratches were 5, 0.5, and 0.5 mm, respectively. For the short-circuit faults, a one-turn fault was made in the stator winding. For the broken rotor bar fault, a hole was drilled into the rotor bar. The dimensions of the rotor are shown in Table 1. The diameter and the depth of the hole are 8 mm and 9 mm, respectively, which can cut one rotor bar. These faults are shown in Fig. 3.

Creating and maintaining single short-circuit faults are difficult because large current flows due to short circuits damage the components in the nearby winding. Consequently, the

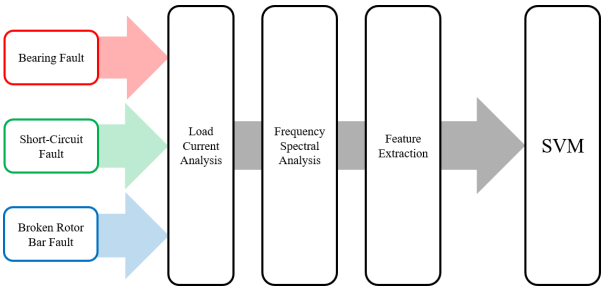

FIGURE 4. Diagnosis procedure of this study.

single-turn fault is extended to two or more turn short-circuit faults. This may cause harmful electrical machine fault due to the sudden increase in temperature and the large current flow through the winding. Thus, we carefully handled the fabrication and maintenance of the single short-circuit faults by reducing the measurement time.

Figure 4 shows the diagnosis procedure of this study. First, the time-domain waveform of the load current of the U phase for each kind of fault was recorded. Second, the frequency spectrum was obtained through fast Fourier transformation. Then, the specific spectrum components of the load current were extracted. Finally, the spectrum components for each kind of fault were merged, including the healthy motor, and diagnosed using SVM.

Two healthy IMs of the same rating were prepared for this experiment. One of the motors was for the bearing and short-circuit faults. The other one was for the broken rotor bar fault. First, the load current spectra of the two healthy motors were measured. Second, the bearing fault was introduced to the bearing of one of the healthy motors. After the measurement using the bearing fault, the faulty bearing was replaced with a healthy one, followed by the introduction of a short-circuit. The broken rotor bar was then introduced to the other healthy motor.

III. LOAD CURRENT ANALYSIS

A. FREQUENCY SPECTRUM

Figure 5 shows the frequency spectra comparison between the healthy and faulty cases for each class of faults. The rotation speed was 1780 min^{-1}. The amplitude was normalized to a maximum frequency component of 0 dB. The frequency resolution was 0.76 Hz according to the sampling theory. The healthy spectra of Fig. 5(a–c) are slightly different from that of Fig. 5(d). This was because the motor for the bearing and short-circuit faults was different from that for the broken rotor bar fault. Clear amplitude differences were observed at the frequencies of 30- and 90-Hz between the healthy and faulty cases of each class of faults. The amplitude differences at the frequencies of 120, 150 and 180 Hz were observed for bearing hole, bearing scratch and short-circuit. In this study, the 30- and 90-Hz components were used as the features for the SVM because those components differ between healthy and faulty cases for all classes of faults.

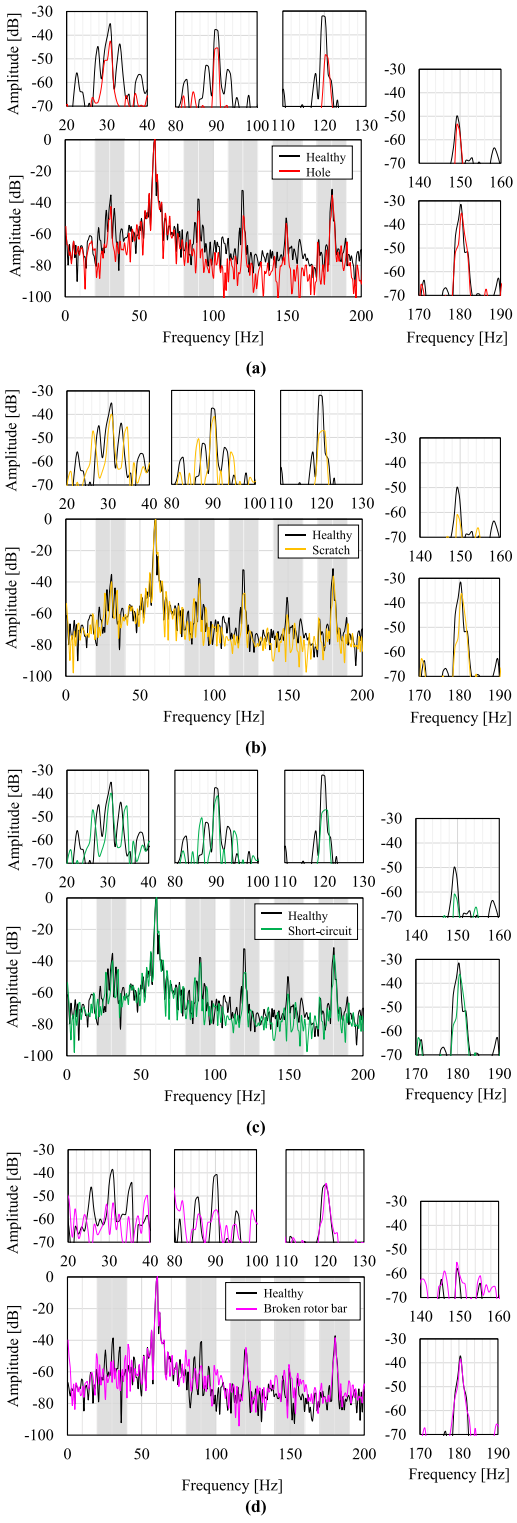

FIGURE 5. Frequency spectrum of the healthy and faulty cases on the bearing at a rotation speed of 1780 min −1. (a) Healthy, bearing (hole), (b) healthy, bearing (scratch), (c) healthy, short circuit, and (d) healthy, broken rotor bar. The hatched range is enlarged as shown in the surrounding figures.

The origin of the amplitude differences for the bearing and short-circuit faults is explained by the axial stray flux, which leaks from the stator windings in IMs [38], [39]. The

stator winding picks up the stray flux. The current with the corresponding frequency components is induced in the load current spectra. The stray flux has a sideband frequency component F_B as follows:

$$F_B = F_L \pm F_R$$

where F_L and F_R are the frequencies of the power supply and rotor rotation, respectively. The F_L is 60 Hz in this study. Meanwhile, F_R is given by

$$F_R = (1 - s) F_L / p$$

where s and p are the rotor slip and the number of pole pairs, respectively. The slip s is

$$s = (N_s - N) / N_s$$

where N_s and N are the synchronous and rotor rotation speeds, respectively. In our experimental setup, p and N_s are 2 and 1800 min^{-1}, respectively. N is 1765, 1770, 1775, and 1780 min^{-1}. Thus, F_R is 29.66–29.41 Hz. Therefore, F_B is the same as the experimentally observed first-order sidebands (30 and 90 Hz), considering the frequency resolution of our setup (0.76 Hz). Meanwhile, the broken rotor bar faults were diagnosed by the twice slip frequency sideband $F_L(1 - 2s)$ [38], [39], which was different from the sideband component F_B. Nevertheless, in this study, the sideband frequency components F_B were used for the broken rotor bars as well as the bearing and short-circuit faults because this study aims to diagnose multiple classes of faults using a common diagnosis method, and the amplitude difference at the sideband components F_B was observed even for the broken rotor bar fault.

Even in the case of the bearing, the origin of sideband components is due to the change of the stray flux affected by the bearing faults on the surface of the outer raceway of the bearing. In this study, the bearing fault are not penetrating through the outer raceway. Practically, previous research works reported that the outer raceway faults of the bearing affect the stator current [40], [41]. Thus, the effect of bearing scratch on the outer surface of outer raceway on the stator current is conceivable.

B. TWO-DIMENSIONAL ANALYSIS

Initially, the features for the SVM were mapped using the amplitudes of 30- and 90-Hz two-dimensionally, as shown in Fig. 6. All the data for the four rotation speeds (1765, 1770, 1775, and 1780 min^{-1}) were combined. For the healthy case, the data of the healthy motor used for the bearing and short-circuit faults were plotted. The reproducibility of the features for the two healthy motors was verified in advance. The difference in the feature distribution between each kind of fault was observed. However, feature overlapping was observed, which can degrade the diagnosis accuracy rates. Thus, the overlapping should be improved.

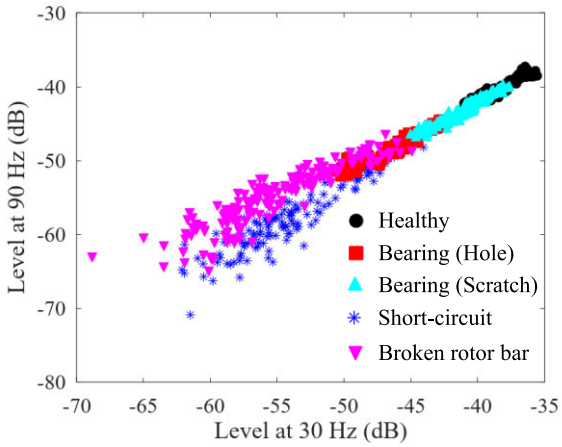

FIGURE 6. Two-dimensional feature distribution. Circles, squares, triangles, asterisks, and inverted triangles show the healthy, bearing (hole), bearing (scratch), short-circuit, and broken rotor bar cases, respectively.

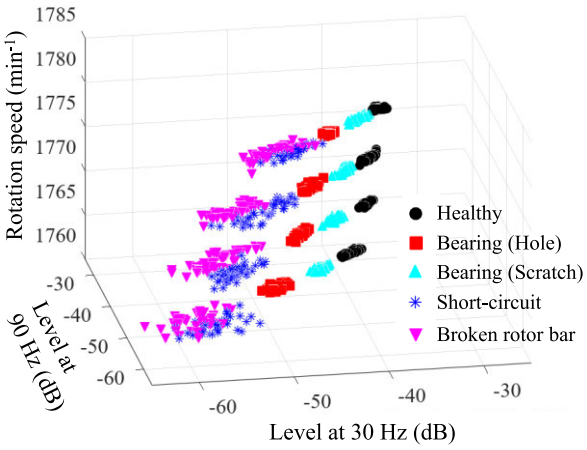

FIGURE 7. Three-dimensional feature distribution. Circles, squares, triangles asterisks and inverted triangles show healthy, bearing (hole), bearing (scratch) short-circuit and broken rotor bar, respectively.

C. THREE-DIMENSIONAL ANALYSIS

Next, a three-dimensional analysis was performed to avoid feature overlapping. The higher-order spectral components such as 120- and 150-Hz were candidates for the additional features. However, these higher-order components did not improve the overlapping according to our initial investigation. Meanwhile, the rotation speed could be an effective additional feature to improve the overlapping [42]. Thus, three-dimensional mapping using the rotation speed as the third feature to improve the feature overlapping was performed in this study. The feature distributions are shown in Fig. 7. The overlapping of feature distributions among each kind of fault was improved in comparison with that in Fig. 6. The features of 30- and 90-Hz for all kinds of faults increased as the rotation speed increased. Meanwhile, feature overlapping was still observed. Especially, the overlapping of the short-circuit and the broken rotor bar was large. Thus, SVM can be

TABLE 2. Diagnosis accuracy.

Fault class	Kind of diagnosis	Accuracy rate (%)
Healthy, bearing (hole)	(i)	100
Healthy, bearing (scratch)		99.41
Healthy, short circuit		100
Healthy, broken rotor bar		100
Healthy, bearing (hole)	(ii)	90.62
Bearing (scratch)		
Short circuit, broken rotor bar		

used for effective diagnosis even in the presence of a slight difference in feature overlapping.

IV. DIAGNOSIS USING SVM

A. DIAGNOSIS PROCEDURE

In this study, the diagnoses were performed using SVM as the ML algorithm. The SVM is an algorism that finds the hyperplane functions in feature distributions. The hyperplane is determined to maximize the distance between the plane and the features. The hyperparameters C and γ are swept to maximize the accuracy rate. The hyperparameters are swept in the range of $10^{-10} \leq C \leq 10^{10}$ and $10^{-10} \leq \gamma \leq 10^{10}$. The accuracy rate in this study is defined as

$$\textit{Accuracy rate}(\%) = \frac{\textit{Number of data diagnosed properly}}{\textit{Total number of data used in diagnosis}} \times 100$$

In this study, 70% and the remaining 30% of the data were used as the training data and test data, respectively. The number of data for each kind of fault and rotation speed is 40.

Two kinds of diagnoses were performed in this study: (i) the diagnosis considering only one specific class of faults and (ii) the diagnosis to identify the class of the faults considering all classes of faults.

B. DIAGNOSIS RESULTS

Figure 8 shows the parameter dependence of the accuracy rates on the hyperparameters C and γ. The color bars show the accuracy rates. Figure 8 (a)–(d) and (e) represent the diagnoses (i) and (ii), respectively. The accuracy rate strongly depended on the hyperparameters. The optimized parameters for all the diagnoses were $C = 2^{-6}$ and $\gamma = 2^{-8}$.

First, diagnosis (i) considering only one specific class of faults was performed. Table 2 shows the accuracy rates. High accuracy rates of more than 90% were obtained for all the diagnoses. Notably, the accuracy rate of the diagnosis of the bearing (hole), short-circuit, and broken rotor bar was 100%. This was because the feature overlapping in these cases was less than that of the bearing (scratch) case, as shown in Fig. 7. Thus, high accuracy rates can be obtained by assuming the class of faults.

Then, diagnoses for identifying the class of faults were performed. Table 2 shows the accuracy rate. An accuracy rate of 90.62% was obtained. Even though the accuracy rate was slightly lower than that of diagnosis (i), it was still high. Thus, the class of faults can be identified with high accuracy.

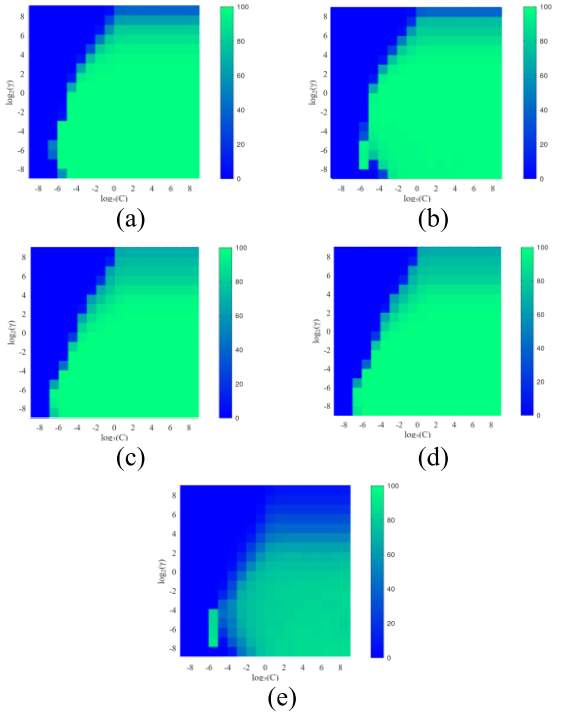

FIGURE 8. Hyperparameter dependence of the accuracy rates in SVM. The color bars show the accuracy rates. (a) Healthy, bearing (hole), (b) healthy, bearing (scratch), (c) healthy, short-circuit, (d) healthy, broken rotor bar, and (e) healthy, bearing (Hole), bearing (scratch), and short-circuit, broken rotor bar.

V. DISCUSSION

In this study, a one-turn short-circuit was introduced to mimic slight faults. The advantage of the present study is that the diagnosis can be performed with high accuracy. The proposed method also gives helpful information at the initial stage of fault to judge if the motor is to be repaired/replaced to avoid fault extension. So far, short-circuit faults have been introduced as multiple-turn short circuits [10], [11]. Because of the high sensitivity of our method, such minor faults were detected.

The accuracy rates for diagnosis (i) were higher than that in diagnosis (ii). Thus, by performing diagnosis (i) after identifying the class of faults using diagnosis (ii), more accurate diagnoses can be expected.

Regarding the computation time of the diagnosis, for the case (i) and the case (ii) which includes the large dataset, the corresponding time consumption was 36 to 40 seconds, and 206 seconds. This mentioned time includes the tuning time of gamma and cost parameters. Also, the computation time depends on the configuration of the PC that is used for machine learning. The configuration of the PC is 4 GB RAM, and Core i5 processor.

To elucidate the advantages of the present method, the results are compared with the other machine learning algorithms like k-NN, random forest, decision tree and

TABLE 3. Comparison of accuracies by the other machine learning algorithms.

Algorithms	Fault class	Accuracy rate (%)
k-NN	Healthy, bearing (hole)	81.46
Random forest	Bearing (scratch)	80.39
Decision tree	Short circuit, broken rotor bar	70.03
k-means		72.72
SVM		90.62

k-means. These algorithms are selected because they are commonly used and emerging in case of the motor diagnosis. The diagnosis case (ii) was considered and performed for the comparison because obtaining the high accuracy rate is more difficult than the diagnosis case (i). The accuracies are summarized in Table 3. The accuracy rate of SVM was 90.62%, which is higher than that of other machine learning algorithms. Thus, SVM is suitable to identify the class of the faults.

In Fig. 7, the feature distribution moved upward as the motor rotation speed increased. As explained in Chapter III, the sideband components of the current spectra originate from the change in magnetic flux. As the rotation speed increases, the number of magnetic flux change in unit time increases. Thus, the sideband components increase as the rotation speed increases. The feature distribution shift due to the change in the motor rotation speed interacts with the neighboring feature distribution of the other class when the rotation speed is not considered. As a comparison and to evaluate the necessity of rotation speed as an additional feature, the two-dimensional feature diagnosis was performed using the frequency components of 30- and 90-Hz. The diagnosis accuracy rate of 62.75% was obtained for the case (ii), which is lower than the accuracy rate using three-dimensional features (rotation speed is included). Thus, using the same SVM algorithm, motor rotation speed acts to be an effective feature for obtaining high accuracy rates.

The SVM can deal with more than four features, which can increase the accuracy rate. The higher-order components of the motor current spectra are candidate additional features. Meanwhile, in the case of more than four features, the feature distribution cannot be visualized. The visualization of data helps us in monitoring motor conditions. The SVM can be followed by the operator's decision when a symptom of fault appears in the feature distribution plot. This procedure saves time for diagnosis.

The proposed diagnosis method could be applied even to inverter-driven IMs. Usually, the operation frequency of inverters is a few kilohertz, which is higher enough than the motor rotation speed. Thus, the sideband frequency components in the load current are not affected by the operation frequency of the inverter.

VI. CONCLUSION

In this paper, diagnoses for classifying major classes of faults were proposed. Slight faults were introduced artificially. The diagnoses were performed by SVM using sideband components in the stator current and the motor rotation speed as the features. In this study, the classes of faults were successfully diagnosed even though feature overlapping between different classes of faults was observed. Although the faults used to imitate faults in initial stage were minor, high accuracy rates were still obtained. The capability to classify the faults and high diagnosis accuracy prove the robustness and high sensitivity of the method, enabling its practical use in industries. In this study, each class of faults was tested independently. However, these classes of faults can occur simultaneously. The diagnosis of simultaneous multiple classes of faults shall be the focus of future studies.

REFERENCES

[1] P. Albrecht, J. Appiarius, R. McCoy, E. Owen, and D. Sharma, "Assessment of the reliability of motors in utility applications—Updated," *IEEE Trans. Energy Convers.*, vol. EC-1, no. 1, pp. 39–46, Mar. 1986.

[2] S. M. A. Cruz and A. J. M. Cardoso, "Stator winding fault diagnosis in three-phase synchronous and asynchronous motors, by the extended Park's vector approach," *IEEE Trans. Ind. Appl.*, vol. 37, no. 5, pp. 1227–1233, Sep. 2001.

[3] J. S. Hsu, "Monitoring of defects in induction motors through air-gap torque observation," *IEEE Trans. Ind. Appl.*, vol. 31, no. 5, pp. 1016–1021, Sep. 1995.

[4] X. Jin, M. H. Azarian, C. Lau, L. Cheng, and M. Pecht, "Physics-of-failure analysis of cooling fans," in *Proc. Prognostics Syst. Health Manage. Conf.*, May 2011, pp. 1–8.

[5] K. Kudelina, T. Vaimann, B. Asad, A. Rassõlkin, A. Kallaste, and G. Demidova, "Trends and challenges in intelligent condition monitoring of electrical machines using machine learning," *Appl. Sci.*, vol. 11, no. 6, p. 2761, Mar. 2021.

[6] J. Cusidó, L. Romeral, J. A. Ortega, J. A. Rosero, and A. G. Espinosa, "Fault detection in induction machines using power spectral density in wavelet decomposition," *IEEE Trans. Ind. Electron.*, vol. 55, no. 2, pp. 633–643, Feb. 2008.

[7] M. N. Uddin, W. Wang, and Z. R. Huang, "Modeling and minimization of speed ripple of a faulty induction motor with broken rotor bars," *IEEE Trans. Ind. Appl.*, vol. 46, no. 6, pp. 2243–2250, Nov. 2010.

[8] M. Riera-Guasp, J. A. Antonino-Daviu, J. Roger-Folch, and M. P. M. Palomares, "The use of the wavelet approximation signal as a tool for the diagnosis of rotor bar failures," *IEEE Trans. Ind. Appl.*, vol. 44, no. 3, pp. 716–726, May 2008.

[9] H. Nakamura, Y. Yagami, C. Araki, and Y. Mizuno, "Probabilistic diagnosis of broken rotor bar of cage induction motor focused on transition features," *IEEJ Trans. EIS*, vol. 135, no. 6, pp. 679–685, 2015.

[10] G. Stone, "Condition monitoring and diagnostics of motor and stator windings—A review," *IEEE Trans. Dielectr. Elect. Insul.*, vol. 20, no. 6, pp. 2073–2080, Dec. 2013.

[11] Y. J. Kim, S. Hoon Hong, T. Sik Kong, and H. D. Kim, "On-site application of novel partial discharge monitoring scheme for rotating machine," in *Proc. IEEE Electr. Insul. Conf. (EIC)*, Aug. 2015, pp. 85–88.

[12] H. Li, R. Li, B. Hu, C. Yan, and Q. Guo, "Application of guided waves and probability imaging approach for insulation damage detection of large generator stator bar," *IEEE Trans. Dielectr. Electr. Insul.*, vol. 22, no. 6, pp. 3216–3225, Dec. 2015.

[13] E. Wiedenbrug, G. Frey, and J. Wilson, "Early intervention," *IEEE Ind. Appl. Mag.*, vol. 10, no. 5, pp. 34–40, Sep. 2004.

[14] H. Nakamura and Y. Mizuno, "Probabilistic diagnosis of short-circuit faults and insulation deterioration of stator winding of motor," *IEEJ Trans. Ind. Appl.*, vol. 132, no. 2, pp. 258–267, 2012.

[15] F. Perisse, P. Werynski, and D. Roger, "A new method for AC machine turn insulation diagnostic based on high frequency resonances," *IEEE Trans. Dielectr. Electr. Insul.*, vol. 14, no. 5, pp. 1308–1315, Oct. 2007.

[16] S. Savin, S. Ait-Amar, and D. Roger, "Turn-to-turn capacitance variations correlated to PDIV for AC motors monitoring," *IEEE Trans. Dielectr. Electr. Insul.*, vol. 20, no. 1, pp. 34–41, Feb. 2013.

[17] S. Das, P. Purkait, C. Koley, and S. Chakravorti, "Performance of a load-immune classifier for robust identification of minor faults in induction motor stator winding," *IEEE Trans. Dielectr. Electr. Insul.*, vol. 21, no. 1, pp. 33–44, Feb. 2014.
[18] H. Nakamura, S. E. Pandarakone, and Y. Mizuno, "A novel approach for detecting broken rotor bar around rated rotating speed using frequency component and clustering," *IEEJ Trans. Electr. Electron. Eng.*, vol. 11, no. S2, pp. S116–S122, Dec. 2016.
[19] H. Nakamura, "Probabilistic diagnosis of short circuit fault of motor on the basis of feature distribution," *IEEJ Trans. Ind. Appl.*, vol. 130, no. 9, pp. 1059–1066, 2010.
[20] W. Zhou, B. Lu, T. G. Habetler, and R. G. Harley, "Incipient bearing fault detection via motor stator current noise cancellation using Wiener filter," *IEEE Trans. Ind. Appl.*, vol. 45, no. 4, pp. 1309–1317, Jul. 2009.
[21] M. Delgado, G. Cirrincione, A. Garcia, J. A. Ortega, and H. Henao, "A novel condition monitoring scheme for bearing faults based on curvilinear component analysis and hierarchical neural networks," in *Proc. XXth Int. Conf. Electr. Mach.*, Sep. 2012, pp. 2472–2478.
[22] X. Jin, M. Zhao, T. W. S. Chow, and M. Pecht, "Motor bearing fault diagnosis using trace ratio linear discriminant analysis," *IEEE Trans. Ind. Electron.*, vol. 61, no. 5, pp. 2441–2451, May 2014.
[23] M. Elforjani and S. Shanbr, "Prognosis of bearing acoustic emission signals using supervised machine learning," *IEEE Trans. Ind. Electron.*, vol. 65, no. 7, pp. 5864–5871, Jul. 2018.
[24] M. He and D. He, "Deep learning based approach for bearing fault diagnosis," *IEEE Trans. Ind. Appl.*, vol. 53, no. 3, pp. 3057–3065, May/Jun. 2017.
[25] H. Nakamura, K. Asano, S. Usuda, and Y. Mizuno, "A diagnosis method of bearing and stator fault in motor using rotating sound based on deep learning," *Energies*, vol. 14, no. 5, p. 1319, Mar. 2021.
[26] L. Frosini, C. Harlişca, and L. Szabó, "Induction machine bearing fault detection by means of statistical processing of the stray flux measurement," *IEEE Trans. Ind. Electron.*, vol. 62, no. 3, pp. 1846–1854, Mar. 2015.
[27] C. Jiang, S. Li, and T. G. Habetler, "A review of condition monitoring of induction motors based on stray flux," in *Proc. IEEE Energy Convers. Congr. Expo. (ECCE)*, Oct. 2017, pp. 5424–5430.
[28] R. R. Schoen, B. K. Lin, T. G. Habetler, J. H. Schlag, and S. Farag, "An unsupervised, on-line system for induction motor fault detection using stator current monitoring," *IEEE Trans. Ind. Appl.*, vol. 31, no. 6, pp. 1280–1286, Nov. 1995.
[29] J. Rosero, L. Romeral, E. Rosero, and J. Urresty, "Fault detection in dynamic conditions by means of discrete wavelet decomposition for PMSM running under bearing damage," in *Proc. 24th Annu. IEEE Appl. Power Electron. Conf. Expo.*, Feb. 2009, pp. 951–956.
[30] A. Picot, Z. Obeid, J. Regnier, P. Maussion, S. Poignant, and O. Darnis, "Bearing fault detection in synchronous machine based on the statistical analysis of stator current," in *Proc. 38th Annu. Conf. IEEE Ind. Electron. Soc. (IECON)*, Oct. 2012, pp. 3862–3867.
[31] Z. Obeid, S. Poignant, J. Regnier, and P. Maussion, "Stator current based indicators for bearing fault detection in synchronous machine by statistical frequency selection," in *Proc. 37th Annu. Conf. IEEE Ind. Electron. Soc. (IECON)*, Nov. 2011, pp. 2036–2041.
[32] J. L. H. Silva and A. J. M. Cardoso, "Bearing failures diagnosis in three-phase induction motors by extended Park's vector approach," in *Proc. 31st Annu. Conf. IEEE Ind. Electron. Soc. (IECON)*, Nov. 2005, p. 6.
[33] R. R. Obaid, T. G. Habetler, and J. R. Stack, "Stator current analysis for bearing damage detection in induction motors," in *Proc. 4th IEEE Int. Symp. Diag. Electr. Mach., Power Electron. Drives (SDEMPED)*, 2003, pp. 182–187.
[34] A. Garcia-Perez, R. de Jesus Romero-Troncoso, E. Cabal-Yepez, and R. A. Osornio-Rios, "The application of high-resolution spectral analysis for identifying multiple combined faults in induction motors," *IEEE Trans. Ind. Electron.*, vol. 58, no. 5, pp. 2002–2010, May 2011.
[35] M. Messaoudi and L. Sbita, "Multiple faults diagnosis in induction motor using the MCSA method," *Int. J. Signal Process.*, vol. 1, no. 3, May 2010.
[36] M. Z. Ali, M. N. S. K. Shabbir, X. Liang, Y. Zhang, and T. Hu, "Machine learning-based fault diagnosis for single- and multi-faults in induction motors using measured stator currents and vibration signals," *IEEE Trans. Ind. Appl.*, vol. 55, no. 3, pp. 2378–2391, May/Jun. 2019.
[37] S. Samanta, J. N. Bera, and G. Sarkar, "KNN based fault diagnosis system for induction motor," in *Proc. 2nd Int. Conf. Control, Instrum., Energy Commun. (CIEC)*, Jan. 2016, pp. 304–308.
[38] W. T. Thomson and M. Fenger, "Current signature analysis to detect induction motor faults," *IEEE Ind. Appl. Mag.*, vol. 7, no. 4, pp. 26–34, Jul. 2001.
[39] S. B. Lee, J. Shin, Y. Park, H. Kim, and J. Kim, "Reliable flux-based detection of induction motor rotor faults from the fifth rotor rotational frequency sideband," *IEEE Trans. Ind. Electron.*, vol. 68, no. 9, pp. 7874–7883, Sep. 2021.
[40] K. C. Deekshit Kompella, M. Venu Gopala Rao, and R. Srinivasa Rao, "Bearing fault detection in a 3 phase induction motor using stator current frequency spectral subtraction with various wavelet decomposition techniques," *Ain Shams Eng. J.*, vol. 9, no. 4, pp. 2427–2439, Dec. 2018.
[41] S. E. Pandarakone, Y. Mizuno, and H. Nakamura, "Evaluating the progression and orientation of scratches on outer-raceway bearing using a pattern recognition method," *IEEE Trans. Ind. Electron.*, vol. 66, no. 2, pp. 1307–1314, Feb. 2019.
[42] H. Nakamura and Y. Mizuno, "Diagnosis for slight bearing fault in induction motor based on combination of selective features and machine learning," *Energies*, vol. 15, no. 2, p. 453, Jan. 2022.

KENICHI YATSUGI was born in Yamaguchi, Japan, in 1987. He received the Bachelor of Engineering (B.E.) and Master of Engineering (M.E.) degrees in applied physics from Osaka University, Japan, in 2010 and 2012, respectively. He is currently a Graduate Researcher with the Graduate School of Engineering, Nagoya Institute of Technology. He engages in the fault diagnosis of electrical machines.

SHRINATHAN ESAKIMUTHU PANDARAKONE was born in Nagercoil, India. He received the Bachelor of Engineering (B.E.) degree in electrical and electronics engineering from Anna University, India, in 2014, the Master of Science (M.Sc.) degree from the Department of Engineering Physics, Electronics and Mechanics, Nagoya Institute of Technology, Japan, in 2017, and the Doctor of Engineering (Dr.Eng.) degree from the Department of Electrical and Mechanical Engineering, Nagoya Institute of Technology, in 2019. His research interests include fault diagnosis of electrical machines, condition monitoring, and failure detection of low-voltage facilities. During his bachelor's course, he was honored for his achievements and performances.

YUKIO MIZUNO (Member, IEEE) was born in Nagoya, Japan, in 1958. He received the B.Sc., M.Sc., and Ph.D. degrees in electrical engineering from Nagoya University, Nagoya, in 1981, 1983, and 1986, respectively. Currently, he is a Professor with the Graduate School of Engineering, Nagare College, Nagoya Institute of Technology. He has been engaged in research on electrical insulation diagnosis, high-voltage insulation, superconducting power cables, quantification of power frequency electric and magnetic fields, among others.

HISAHIDE NAKAMURA (Member, IEEE) was born in Yamaguchi, Japan, in 1971. He received the B.E. and M.E. degrees in electrical and computer engineering from Nagoya Institute of Technology, in 1995 and 1997, respectively, and the Ph.D. degree in electrical engineering from Nagoya University, in 2002. From 1997 to 1999, he worked with FANUC Ltd. In 2002, he joined TOENEC Corporation. His research interest includes fault diagnoses of electrical machines.